1
9-18-78

CONF-780834--4

FUSION WELDING OF IRRADIATED AISI 304L STAINLESS STEEL TUBINGS

by

M. M. Hall, Jr., A. G. Hins, J. R. Summers, and D. E. Walker

Prepared for

Fifth Bolton Landing Conference on
Weldments-Physical Metallurgy and Failure Phenomena

Bolton Landing, Lake George, New York

August 27-30, 1978

ARGONNE NATIONAL LABORATORY, ARGONNE, ILLINOIS

Operated under Contract W-31-109-Eng-38 for the
U. S. DEPARTMENT OF ENERGY

Fusion Welding of Irradiated AISI 304L Stainless Steel Tubing*

M. M. Hall, Jr., A. G. Hins, J. R. Summers, and D. E. Walker

Materials Science Division
ARGONNE NATIONAL LABORATORY
Argonne, Illinois 60439

ABSTRACT

Fast reactor irradiated AISI 304L stainless steel tubing was fusion-welded using conventional inert gas-tungsten arc welding (GTAW) procedures which were adapted for remote operation. Metallographic examination of weld joints sometimes revealed porosity in the weld zone and cracks at the tube inner wall within the heat-affected zone. A stress analysis was performed to evaluate these defects as sites for weld failure and to establish procedures for the detection and rejection of weld joints likely to fail in service.

INTRODUCTION

An in-reactor creep experiment that is currently being conducted by Argonne National Laboratory in Experimental Breeder Reactor (EBR)-II uses gas-pressurized creep capsules that were fabricated from sections of previously irradiated stainless steel tubing. Since there appeared to be no published accounts of applicable past welding experience, we decided to adapt conventional welding procedures to weld end fittings to the irradiated specimen tubes. One purpose of this paper is to describe the weld-related defects discovered during metallographic examination of qualification-weld samples. Since these weld defects occurred infrequently, no attempt was made to determine why they occurred or to discover ways to control or eliminate them. We relied instead on nondestructive techniques to detect the occurrence of defects, and on proof-tests to reject creep capsules susceptible to weld-related failures. A further purpose of this paper is to present the results of the stress analyses that were performed to evaluate the observed defects as sources of creep-capsule failure. The

---

*Work supported by the U.S. Department of Energy.

results of this evaluation were used to set limits on the size of acceptable defects and to determine the details of the proof-testing procedures. Finally, we speculate on the causes of the observed defects and discuss modifications of the weld-joint design and welding procedures that may improve the reliability of fusion welds of irradiated materials.

MATERIALS AND PROCEDURES

Materials

The AISI 304L solution-annealed stainless steel tubing used in this work had previously been used to encapsulate EBR-II reactor-fuel pins as part of a driver-fuel surveillance program. The chemical composition of the as-fabricated tubing material was analyzed by wet-chemistry techniques, and the results are given in Table 1. Tube sections with a length of 1.375 in. (34.93 mm), a nominal outer diameter of 0.290 in. (7.37 mm), and a wall thickness of 0.020 in. (0.51 mm) were taken from capsule tubes that had previously been irradiated at temperatures between 849°F (454°C) and 908°F (487°C) to integrated fast fluxes between 1.38×10^{22} n/cm^2 and 7.51×10^{22} n/cm^2 (E > 0.1 Mev). The tubing end plugs were fabricated from AISI 304 stainless steel with the chemical composition given in Table 1.

Table 1. Chemical Composition of Specimen Tubes and End Fittings

	Element (wt%)										
	C	Mn	P	S	Si	Ni	Cr	Ti	Cu	Mo	Co
Tube (AISI 304L)	0.03	1.37	0.01	0.007	0.62	9.26	18.3	0.02	0.074	0.02	0.05
End Fitting (AISI 304)	0.074	1.73	0.034	0.009	0.53	9.35	18.35	-	0.38	0.43	0.15

Weld Procedure

Conventional inert gas-tungsten arc welding (GTAW) procedures were adapted for remote operation. The tubing, end-fitting, and tungsten-electrode configurations are shown in Fig. 1. Welding is accomplished remotely in a shielded cell by fusing the tube and end fitting (without filler metal) while rotating them horizontally under a He-30% Ar cover gas. The welding current and the rotation speed of the work piece were preselected and automatically controlled. Weld parameters are summarized in Table 2. Split copper chills were placed 0.200 in. (5.08 mm) from the tube-end fitting interface to prevent overheating of the tubing. The weld current used for the irradiated tubing (Table 2) was found to be one to two amperes less than that required to produce similar welds with unirradiated tubing.

Inspection Techniques

Metallographic examination of weld joints was accomplished with a remotely operated optical microscope. Nondestructive examination was accomplished by means of x-ray radiography. Unwanted film exposure, caused by gamma radiation emitted from the irradiated tubing, was minimized by using low-speed film and short contact time of the part with the film.

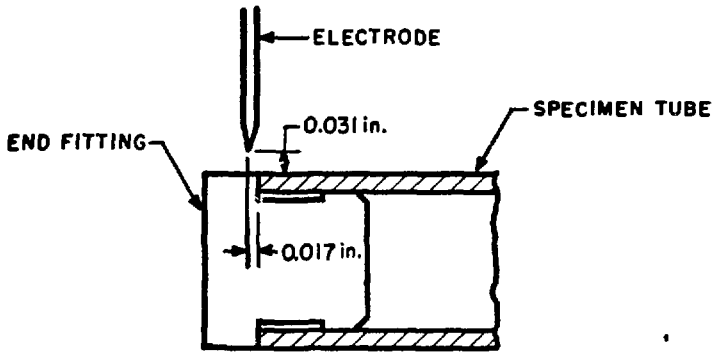

Fig. 1 Tungsten Electrode Placement Relative to Specimen Tube and End Fitting.

Table 2. Weld Parameters

Weld Current	21 A
Final Current	Slope decay to 9 A
Rotation Speed	11 r/min
Rotation Delay	0.1 S
Weld Overlap	40° minimum
Shield Gas	70% He/30% Ar mixture
Gas Flow Rate	20 ft^3/h (9.4 l/s)
Electrode	0.040 in. (1.0 mm) EWTH-2, 25° included angle, 0.010 in. (0.3 mm) blunt end
Weld Chills	Two-piece split copper rings 0.200 in. (5.08 mm) from tubing-end fitting interface

Pressure Prooftest

All creep capsules were prooftested at the design operating pressure and temperature. Each helium-pressurized creep capsule was placed in a vacuum furnace at room temperature, heated to 932°F (500°C), and held for 2 h; during this time, a helium mass spectrometer was used to detect specimen leaks.

RESULTS OF WELD TESTS AND INSPECTIONS

Two weld-related defects were observed during metallographic examination of developmental welds. First, spherical cavities or pores were found in the weld zone; these are shown schematically in Fig. 2, which illustrates typical weld-joint geometry. Pores were, in most cases, <0.001 in. (0.025 mm) in diameter and were found most often near the end fitting-weld zone interface. However, pores were occasionally found near the specimen tube-weld zone interface and could be as large as 0.010 in. (0.25 mm) in diameter. Pores shown in Fig. 3 are typical of those observed most often. The sensitivity of our radiographic inspection technique was found to be sufficient for the detection of pores with diameters

≳0.004 in. (0.10 mm). Of 56 welds inspected by radiography, only one was rejected because of detectable pores too near the tube-weld zone interface.

A second type of weld-related defect consists of cracks, which appear to be grain-boundary separations, along the specimen tube's inner diameter within the heat-affected zone, i.e., within approximately 0.150 in. (3.81 mm) of the tube-weld zone interface. The cracks shown schematically in Fig. 2 and visible in Fig. 4 are typical. These cracks were observed in only 2 of 11 developmental welds examined. Since, however, these defects are very likely sites for creep-capsule failure and are not easily detected by nondestructive examination, all creep capsules were pressure prooftested by means of the test described above. Of 29 creep capsules so tested, only two failures were noted. One failure occurred as a minute pinhole leak near the tube-weld zone interface. The other failure occurred as a catastrophic rupture that included a circumferential separation of the tube and end fitting, also very near the tube-weld interface, as shown in Fig. 5. Both failures appear to be associated with the heat-affected zone. The difference between the pinhole failure and the rupture is probably due to the somewhat higher initial pressure in the latter case.

STRESS ANALYSIS

Porosity

Porosity was observed to occur most often near the end fitting-weld zone interface. It is clear that porosity in this region (Fig. 2, region A) should have little effect on weld integrity. However, the porosity that sometimes occurs near the specimen tube-weld zone interface (region B) reduces the effective weld-tube wall thickness so that abnormally high stresses are expected in this region when the tube is internally pressurized. We could find no solution to this stress problem in the literature. However, a solution to the problem of a strip perforated with a cylindrical hole and subjected to tension, bending, and shear is available.[1,2] We are, therefore, able to obtain an approximate (and, we think, conservative) idea of the actual stresses if we apply the perforated-strip solutions to the longitudinal tube-wall element shown in Fig. 6. This element is taken through the weld zone so as to include a cross section of a spherical pore. That the stresses obtained in this way are conservative can be shown by comparing the solution for a cylindrical hole in a strip of infinite width under uniaxial tension T with that of a spherical hole in a tensile bar of infinite diameter, also under uniaxial tension T. The maximum tensile stress at the edge of the cylindrical hole is 3T, while the maximum tensile stress at the surface of the sphere[3] is 2T. We therefore expect that our approximate solution will be conservative by the ratio of these solutions.

We consider the pore to be located as shown in Fig. 2 and look to Ref. 2 for the bending stress σ_{xx} and the shear stress σ_{xy} across the section mn, caused by the bending moment M and the shearing force Q, respectively. In addition, Ref. 2 gives us the tensile stress $\sigma_{\phi\phi}$ at the edge of the hole as a result of M and Q. To these stresses we must add pr/2t, which is the uniform axial membrane stress for a thin-walled tube of radius r and wall thickness t under internal pressure p. Figure 7 shows the resulting axial stress distribution through section mn (see Fig. 2), from the tube midwall to the tube inner diameter, for the case of no pore and for pores having diameter to wall-thickness ratios R = 0.2, 0.3, 0.4, and 0.5. Note that for R > 0.2, the axial stress at the pore surface becomes greater than the maximum stress that occurs at the tube

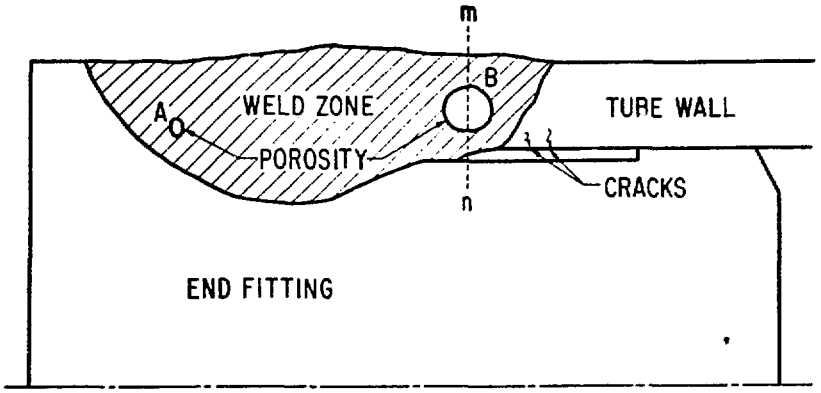

Fig. 2 Typical Weld-joint Geometry Showing Location of Weld-related Defects.

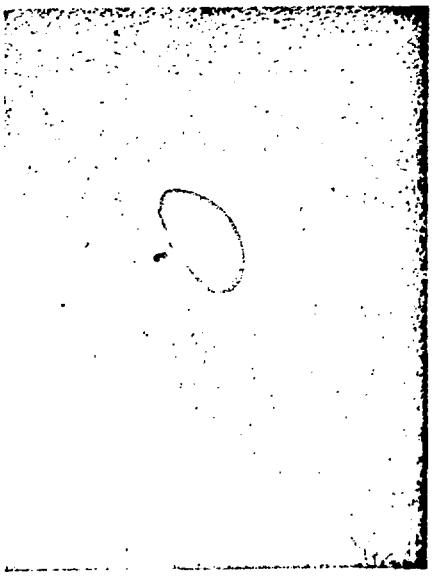

Fig. 3 Porosity in GTAW Fusion Weld of Irradiated AISI 304L Tube. 200X

Fig. 4 Grain-boundary Cracks Appearing in Heat-affected Zone during GTAW Fusion Welding of Irradiated AISI 304L Tube. 500X

Fig. 5 Creep Capsule Failure that Appears to Have Been Initiated in Heat-affected Zone.

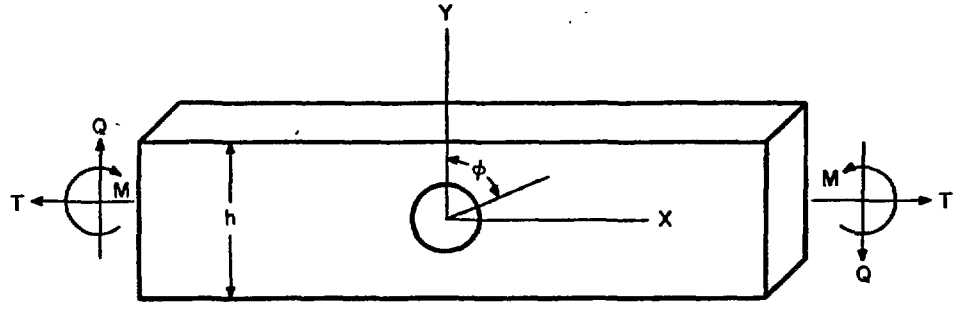

Fig. 6 Longitudinal Section of Specimen Tube Wall, Taken to Include a Cross Section of a Weld Pore.

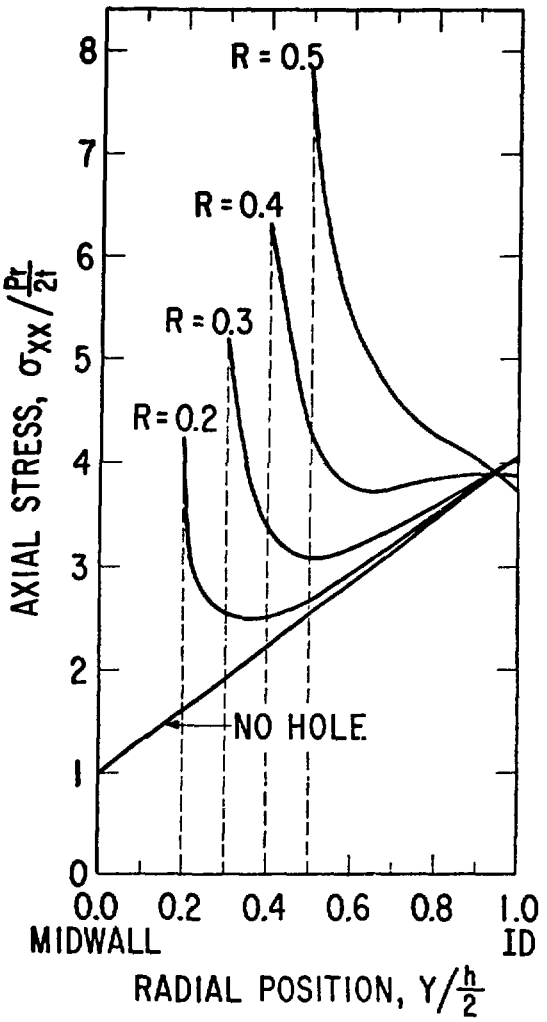

Fig. 7 Normalized Axial Stress Distribution Through Tube-wall Section mn (Fig. 2).

inner diameter when no pore is present. Figure 8 shows the tensile stress $\sigma_{\phi\phi}$ at the surface of the pore as a function of the angle ϕ (Fig. 6). We see that the maximum value of $\sigma_{\phi\phi}$ occurs for $\phi \approx 189°$-$190°$; this maximum value is only slightly greater than the values given in Fig. 7 [$\sigma_{\phi\phi}$ (180°) = σ_{xx} of Fig. 7].

Fig. 9 shows the distribution of the shear stress σ_{xy} through the section mn (see Fig. 2), from the tube midwall to the tube inner diameter, for the case of no pore and for pores with R = 0.2, 0.3, 0.4, and 0.5. We see that even when R is as large as 0.5, the maximum shear stress is only 0.72 of the pressure stress pr/t, which is the hoop membrane stress, σ_θ, for a pressurized thin-walled tube. Since generalized or uniform yielding occurs for a capped-end tube only when $\sigma_\theta > 1.15\ \sigma_y$ (where σ_y is the yield stress), yielding in the specimen gauge section will occur before σ_{xy} can cause yielding in section mn, even when pores with R as large as 0.5 are present.

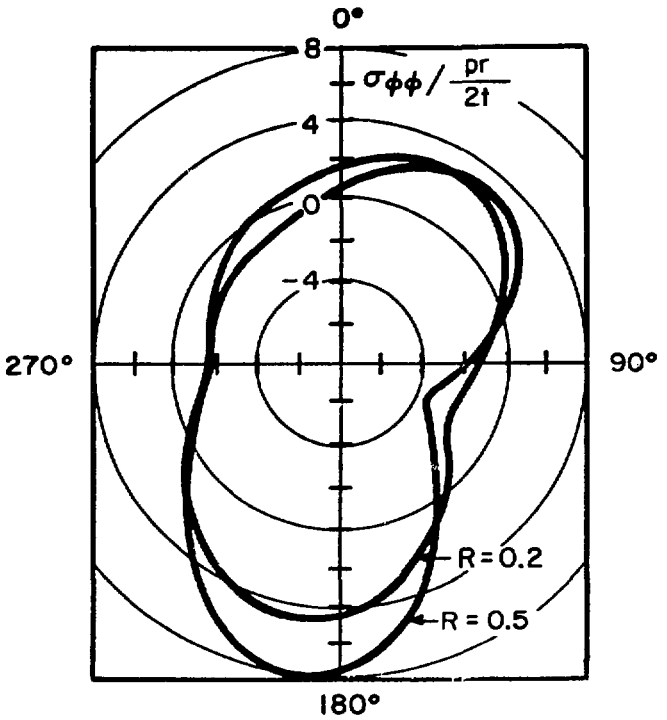

Fig. 8 Normalized Tangential Stress Distribution at a Pore Surface.

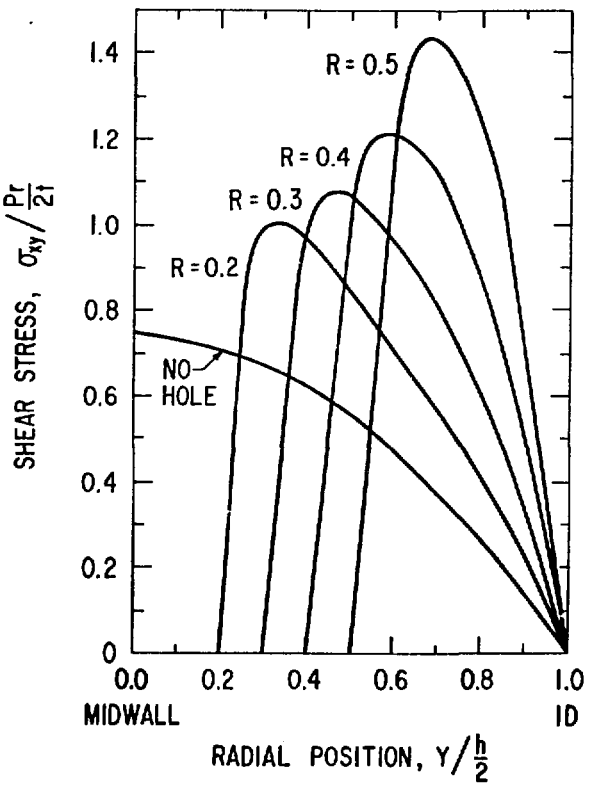

Fig. 9 Normalized Shear-stress Distribution Through Tube-wall Section mn (Fig. 2).

Cracks

Cracks that occur near the weld joint on the inner diameter of a pressurized tube, like ones shown in Fig. 4, are likely sites for initiation of creep-capsule failures, since this region of the tube wall is subjected to large tensile bending stresses. These stresses are caused by the bending moment and shear forces that must be applied to the tube end (which tends to expand circumferentially when the tube is pressurized) in order to prevent diameter discontinuities at the junction of the tube with the rigid end fitting. Solutions for the axial bending stresses, σ_x, and the hoop stresses, σ_θ, may be accomplished by means of cylindrical shell theory.[4] Figure 10 shows solutions for the axial and hoop stresses at the inner and outer tube diameters as a function of a dimensionless distance, βx, from the tube-end fitting interface for an internally pressurized capped-end tube.* For the tubes used in the current study, $\beta = 23.6$ in.$^{-1}$ (0.93 mm^{-1}). Figure 10 shows that the axial stress, σ_{xi}, at the inner diameter can be as large as 3.5 times the uniform midwall stress, $\sigma_x = pr/2t$, and falls to the uniform value at a distance $\beta x = 0.6$, that is, $x = 0.025$ in. (0.64 mm), from the tube-end fitting interface. Therefore, cracks located within this area are particularly likely sites for failure initiation.

Restrained Swelling

An additional source of stress that could in principle cause creep-capsule failure is the mechanical restraint of irradiation-induced swelling.** The restraint comes about when the tubing, which was previously irradiated well beyond the incubation period for the onset of significant swelling, is welded to previously unirradiated, and therefore low-swelling, rigid end fittings. The difference between the swelling rates of the end fittings and that of the irradiated tubing leads to large discontinuity stresses at the tube-end fitting interface. The tube creeps in response to these swelling-induced stresses and a saturation stress level is attained, with the stress magnitude proportional to the ratio of swelling and creep rates. A full solution of this stress problem is presently being considered and will be submitted elsewhere.[5]

Briefly, a conservative solution to this problem, which ignores local reduction of swelling rate caused by thermal annealing of irradiation microstructure in the heat-affected zone, is arrived at by analogy with the linear thermo-elastic solution for stresses caused by a step increase in tube temperature at the tube-end fitting interface. This analogy[6] is possible because the irradiation-induced creep rate is linearly proportional to the applied stress, under temperature and stress conditions relevant to the present discussion. Figure 11 shows solutions for the axial and hoop stresses at the inner and outer tube diameters as a function of βx. Stresses are proportional to the ratio $\Delta\dot{S}/B$, where $\Delta\dot{S}$ is the difference between end-fitting and specimen-tube swelling rates and B is the irradiation-creep coefficient. In-reactor measurements of these quantities[7] indicate that the ratio $\Delta\dot{S}/B$ may be as large as 45,400 psi (313 MPa). Figure 11 shows that in this case, the axial bending stress may be as large as 30,264 psi (209 MPa). We do not believe that stresses this high are attained, since the actual axial variation in swelling rate from the end fitting to the specimen tube, as discussed below, is more gradual than a step increase. We have demonstrated, however, that there is potential for significant stress caused by restrained swelling.

---

*See Ref. 4 for a definition of β.

**Decreases in density accompanied by the formation of voids.

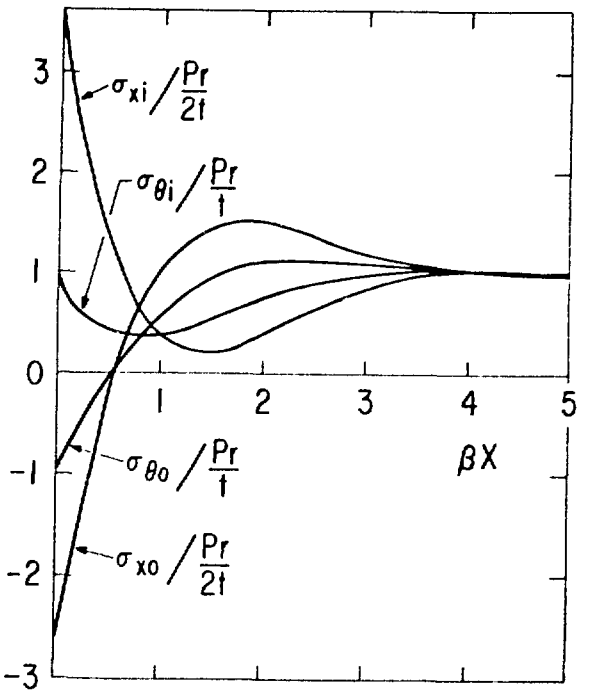

Fig. 10 Axial and Circumferential Discontinuity Pressure-stress Distributions Near the Tube-Weld Zone Interface.

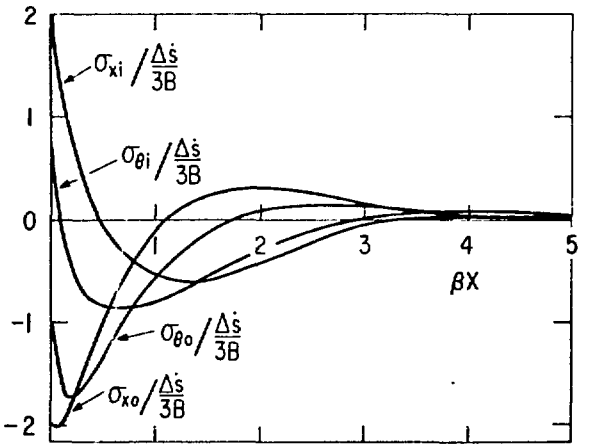

Fig. 11 Axial and Circumferential Swelling-restraint Stress Distributions Near the Tube-Weld Zone Interface.

DISCUSSION

Porosity

Comparison of Figs. 7, 8, and 9 shows that the potentially most damaging stress effect of porosity in the weld zone is the increase in the axial tensile stress that occurs at the tube-end fitting interface from the tube midwall to the inner diameter. When possible, all welds that have pores which either intersect or fall on the tube side of the original tube-end fitting interface should be rejected. However, Fig. 7 suggests that pores with $R < 0.20$ should be acceptable in this region. For $R < 0.20$, the maximum stress caused by the pore is no greater than that expected without the pore. Of course, if the uniform pressure stresses (far from the end fitting) were very low, e.g., less than one-tenth of the stress expected to cause failure in the uniform tube section during the design lifetime, then welds having as much as a 50% reduction in minimum wall thickness caused by porosity might be acceptable. In this case the maximum stress caused by the presence of the pore would be less than ten times the stress expected with no pores present. In any case, Fig. 6 can serve as a guide when deciding which welds to accept or reject.

We conjecture that the occurrence of porosity in fusion welds of our irradiated tubing is due to helium, which is produced during irradiation by (n, α) transmutation reactions, and precipitated and trapped as gas bubbles during the welding process. The feasibility of this explanation is supported by our estimate that, since the He production rate for AISI 304L stainless steel in EBR-II is approximately 6.3×10^{-7} appm/sec, enough He is available within the weld zone to form up to 2000 equilibrium gas bubbles as large as 0.010 in. (0.25 mm) in diameter during the welding of tubing having a fast-neutron exposure of 6×10^{22} n/cm^2 ($E > 0.1$ MeV). However, we do not observe this many bubbles, probably because much of the gas escapes the melt. Other explanations, such as cover-gas entrapment or vaporization of impurities, seem improbable since we made many welds of the same lot of tubing in the unirradiated condition by means of the same weld procedure without seeing any evidence of porosity. Control of porosity caused by He gas release will be difficult, but could perhaps be enhanced by standard techniques such as slower rotational speeds and greater heat input to allow slower cooling and therefore more time for the gas to escape the melt.

Cracks

Of the two types of defects discovered, the grain-boundary separations at the tube inner diameter near the weld zone are the more likely sites for failure. These defects are a particular threat since they are not easily detected. We believe, however, that pressure prooftesting at the design operating temperature is a good technique for elimination of welds that are susceptible to failure. When possible, prooftests should be carried out at pressures above design operating pressures. Although the tubing near the weld zone is softened by the heat of the weld, it is most likely also embrittled by extensive grain-boundary precipitation of He gas.[8] Prooftesting at high pressures should then propagate cracks and eliminate those creep capsules likely to fail in service. Helium embrittlement by precipitation to grain boundaries, coupled with thermal shrinkage of the tube following weld solidification, is in fact the probable cause of the cracks.

If the prooftest temperature is high enough for thermal creep or plastic flow, an additional benefit of the pressure prooftest is that discontinuity stresses may be relieved before insertion of the pressurized creep capsule into the reactor. This may be important since, although a creep capsule may survive the out-of-reactor pressure prooftest at the operating temperature, it may fail in-reactor when swelling-restraint stresses are added to the discontinuity stresses caused by pressure loading alone.

Swelling-restraint stresses, unlike the pressure-induced discontinuity stresses, are not eliminated by creep strain but instead quickly reach a saturation value proportional to the ratio of swelling and creep rates. However, the magnitude of these stresses will not be as large as predicted for a step increase in swelling rate at the tube-end fitting interface, since the actual swelling-rate increase is more gradual. Temperatures in excess of approximately 900°F (482°C) destroy the microstructure responsible for high swelling rate, and cause the full swelling-rate transition to take place over an axial distance within the heat-affected zone. Since the magnitude of swelling-restraint stresses also depends upon the rate of transition along the tube length from the low swelling rates of the unirradiated end fittings to the high swelling rates of the irradiated tubing, swelling-restraint stresses should be reduced by applying procedures which insure a large heat-affected zone. Two procedures that may help are (1) use of no weld chills during the welding process, and (2) application of an annealing heat treatment to the end of the welded tube. As mentioned above, the details of this problem are being considered and are to be reported.

Circumferential collars placed over the heat-affected zone would appear to reduce the probability of capsule failure by lowering the pressure stresses in the area most susceptible to failure by crack initiation and growth. However, these collars would effectively create the step increase in circumferential strain rate discussed above and would therefore insure the maximum possible swelling-restraint stresses, although these would of course occur beyond the heat-affected zone.

Only experience with these various weld designs and procedures will determine which produces the most reliable weld joints. At the time of this writing our creep capsules, which were fabricated by means of the weld procedures described above, have survived 2200 hours in-reactor, without any evidence of failure.

CONCLUSIONS

1. Although the irradiation-induced microstructure of the irradiated tubing will sometimes cause porosity to occur in the weld zone and tube cracks to occur in the heat-affected zone, the nondestructive examination and prooftesting procedures described above can be used to identify and reject those welds likely to fail in service.

2. AISI 304L stainless steel tubing having fast-flux exposures as high as 7.51×10^{22} n/cm^2 (E > 0.1 MeV) may be successfully welded using conventional GTAW fusion welding procedures.

ACKNOWLEDGMENTS

The authors would like to thank F. E. Savoie, who carried out the welding program.

REFERENCES

1. R. C. J. Howland, Proc. R. Soc. , Ser. A 229, 49 (1930).

2. R. C. J. Howland and A. C. Stevenson, Proc. R. Soc. London, Ser. A 232, 155 (1933).

3. S. P. Timoshenko and J. N. Goodier, Theory of Elasticity, 3rd ed. (McGraw-Hill, New York, 1970), pp. 396-398.

4. S. P. Timoshenko and S. Woinowsky-Krieger, Theory of Plates and Shells, 2nd ed. (McGraw-Hill, New York, 1959), pp. 466-501.

5. M. M. Hall, Jr., "Irradiation Swelling-Induced Stresses in a Circumferentially Restrained Circular Cylinder," to be submitted to Nuclear Technology.

6. G. L. Wire and J. L. Straalsund, "A Simple Method for Calculations of Steady-State Creep Rates in Nonconservative Plastic Deformation," Nucl. Technol. 30, 71-76 (1976).

7. L. C. Walters, G. L. McVay, and G. D. Hudman, "Irradiation-Induced Creep in 316 and 304L Stainless Steels," ANS-AIME Intl. Conf. on Radiation Effects in Breeder Reactor Structural Materials, ed. M. L. Bleiberg and J. W. Bennett (1977), 191-207.

8. M. L. Grossbeck, J. O. Stiegler, and J. J. Holmes, "Effects of Irradiation on the Fracture Behavior of Austenitic Stainless Steel," ANS-AIME Intl. Conf. on Radiation Effects in Breeder Reactor Structural Materials, ed. M. L. Bleiberg and J. W. Bennett (1977), 95-116.